Cell. Mol. Life Sci. (2012) 69:299–311
DOI 10.1007/s00018-011-0749-8

Cellular and Molecular Life Sciences

RESEARCH ARTICLE

# Functional characterization of the human myosin-7a motor domain

**Sarah M. Heissler · Dietmar J. Manstein**

Received: 5 January 2011 / Revised: 30 May 2011 / Accepted: 1 June 2011 / Published online: 18 June 2011


**Abstract** Myosin-7a participates in auditory and visual processes. Defects in *MYO7A*, the gene encoding the myosin-7a heavy chain, are causative for Usher syndrome 1B, the most frequent cause of deaf-blindness in humans. In the present study, we performed a detailed kinetic and functional characterization of the isolated human myosin-7a motor domain to elucidate the details of chemomechanical coupling and the regulation of motor function. A rate-limiting, slow ADP release step causes long lifetimes of strong actin-binding intermediates and results in a high duty ratio. Moreover, our results reveal a $Mg^{2+}$-sensitive regulatory mechanism tuning the kinetic and mechanical properties of the myosin-7a motor domain. We obtained direct evidence that changes in the concentration of free $Mg^{2+}$ ions affect the motor properties of human myosin-7a using an in vitro motility assay system. Our results suggest that in a cellular environment, compartment-specific fluctuations in free $Mg^{2+}$ ions can mediate the conditional switching of myosin-7a between cargo moving and tension bearing modes.

**Keywords** Actin · Myosin · Transient kinetics · ATPase · Mangnesium ions

**Abbreviations**

| | |
|---|---|
| *Dd* | *Dictyostelium discoideum* |
| dmADP | Desoxy-mantADP |
| dmATP | Desoxy-mantATP |
| DTT | 1,4-Dithiothreitol |
| EYFP | Enhanced yellow fluorescent protein |
| HEPES | 4-(2-Hydroxyethyl)-1-piperazineethanesulfonic acid |
| LDH | Lactate dehydrogenase |
| mant | N-methylanthraniloyl |
| MOPS | 4-Morpholinepropanesulfonic acid |
| PEP | Phosphoenolpyruvate |
| PK | Pyruvate kinase |
| RPE | Retinal pigment epithelial |
| *Sf*9 | *Spodoptera frugiperda* |
| TRITC | Tetramethylrhodamine isothiocyanate |

S. M. Heissler · D. J. Manstein (✉)
Institut für Biophysikalische Chemie, Medizinische Hochschule Hannover, Carl-Neuberg-Str. 1, 30625 Hannover, Germany
e-mail: manstein.dietmar@mh-hannover.de

S. M. Heissler
e-mail: sarah.heissler@nih.gov

## Introduction

Myosin is a mechanoenzyme that uses actin-activated ATP turnover to power interactions with actin filaments producing force and/or driving directed movement. Class 7 myosins form one of the 12 myosin classes found in humans [1]. They are among the most widely produced myosins in the animal kingdom and display broad tissue expression [2–4]. Two distinct class 7 myosins are produced in humans. The myosin-7a and myosin-7b heavy chains are encoded by *MYO7A* and *MYO7B*, and display distinct kinetic and functional properties. The human myosin-7a heavy chain is composed of the N-terminal motor domain, a neck region with 5 IQ motifs, and a complex tail region. The tail region contains a SAH domain (absent in vertebrate myosin-7b), a ~460 amino acid segment formed by a myosin tail homology 4 (MyTh4) domain and a band 4.1-ezrin-radixin-moesin (FERM) domain, an SH3 domain, and a second, C-terminal MyTH4-FERM tandem domain [2, 5–7]. Myosin-7a

activity is regulated by an interaction between the tip of the tail and the motor domain [8]. Moreover, the SAH domain acts as a lever arm extension [8]. It has been suggested that myosin-7 functions by exerting local tension, especially at the plasma membrane, and moving cargos. Myosin-7a was found to associate with lysosomes and may be involved in lysosome trafficking [9]. However, most studies of myosin-7a function focused on its role in auditory and visual processes.

In the auditory apparatus, myosin-7a is produced in cochlear mechanosensory stereocilia of the hair cells, where it is involved in hair bundle morphogenesis and mechanotransduction [10–12]. Additionally, myosin-7a motor activity contributes to processes such as differentiation and organization of hair cell stereocilia [12]. Within the neuroretina, myosin-7a is involved in the distribution and migration of retinal pigment epithelial (RPE) melanosomes and phagosomes [13, 14], and enables the regulation of opsin transport in retinal photoreceptors [15, 16]. Mutations in *MYO7A* are associated with several forms of inherited deafness and deaf-blindness in both humans and mice [17, 18]. *MYO7A* mutations are causative for hearing impairment and vestibular dysfunction in Usher syndrome type 1B (USH1B), the major cause of deaf-blindness in humans, and are linked to non-syndromic hearing loss (DFNB2, DFNA11) [17, 19]. The murine orthologue of *MYO7A* is causative for the *shaker-1* phenotype [18].

At the protein level, the central SAH domain forms a stable single $\alpha$-helix and acts as a lever arm extension, rather than dimerizing two myosin molecules as previously proposed [8]. Isolated molecules of *Drospohila* myosin-7a are monomeric [8], which raises the possibility that the human orthologue is a single-headed molecular motor as well [20]. The motor properties of human myosin-7a are largely unknown. In the present study, we produced the motor domain of human myosin-7a fused to an artificial lever arm and an EYFP fluorescence marker (M7a). We used construct M7a to analyze the kinetic and functional properties of the myosin-7a motor domain. Our results show that human myosin-7a is a slow motor with a rate-limiting ADP release step from actomyosin and a high affinity for F-actin, even in the presence of ATP. Additionally, we report a $Mg^{2+}$ ion-sensitive regulatory mechanism affecting ATP turnover, ADP release kinetics from actomyosin, and motor activity.

## Materials and methods

### Reagents

TRITC-phalloidin was purchased from Sigma-Aldrich; His antibody and $Ni^{2+}$-NTA were from QIAGEN. Restriction enzymes, polymerases, LR and BP Clonase enzyme mixture, and DNA-modifying enzymes were purchased from MBI-Fermentas, Finnzymes, and Invitrogen. Other enzymes and protease inhibitor cocktail tablets were from Roche Applied Sciences. Standard reagents were from Sigma-Aldrich.

### Construction of baculovirus transfer vectors

The myosin-7a construct was cloned by fusing the human myosin-7a motor domain (amino acids 1–747) with an artificial lever arm (named "2R") and an EYFP fluorescence marker. A C-terminal $His_8$-tag enables $Ni^{2+}$-chelate affinity chromatography. The molecular mass of the fusion construct was calculated to be 142 kDa from amino acid sequence. The human myosin-7a cDNA clone pCMV-Sport6-Myo7a was a generous gift of Dr. D.S. Williams (UCSD School of Medicine, La Jolla, CA). The motor domain of human myosin-7a was subcloned into pGEM-T-Easy using a pair of primers. The motor domain was amplified using the primers 5REC-M7MDH8 (GGG GAC AAG TTT GTA CAA AAA AGC AGG CTC CGG ATC CAT GGT GAT TCT TCA GCA GGG G) and 3REC-M7MDH8 (GGG GAC CAC TTT GTA CAA GAA AGC TGG GTC ATC TCG AGT GTC GGT GAT GGC TTT GTC CCG). The PCR fragment was used in the BP recombination according to the manufacturer (Invitrogen) with the vector pDONR201. The entry vector was used in a LR recombination reaction with the vector pDEST8 according to the manufacturer's instruction. The motor domain construct fused to the 2R-EYFP unit was obtained by insertion of the 2R-EYFP-$His_8$ cassette from the vector pDONR201-2R-EYFP-$His_8$ in frame with the myosin motor domain by digestion with *Xho*I. The transfer vector was confirmed by sequencing.

### Production and preparation of recombinant protein

The myosin fusion protein was overproduced using the baculovirus/*Sf*9 system. Therefore, the transfer vector was transformed in DH10Bac *E. coli* cells to generate recombinant bacmid. Bacmid was isolated and transfected in *Sf*9 insect cells using Cellfectin II (Invitrogen). Recombinant baculovirus was produced as described by the manufacturer. *Sf*9 cells were infected with recombinant baculovirus, collected 72 h *post infectionem* and stored at −80°C.

For purification, cells were lysed [50 mM HEPES (pH 7.3), 300 mM NaCl, 3 mM $MgCl_2$, 2 mM ATP, 10 mM $\beta$-mercaptoethanol, 4 mM imidazole, in the presence of protease inhibitors], ultracentrifuged (138,000×*g*, 35 min) and the extract applied to a $Ni^{2+}$-affinity column. The resin was washed with ATP buffer (25 mM HEPES (pH 7.3), 600 mM NaCl, 0.5 mM ATP, 0.1 mM EGTA, 3 mM $MgCl_2$, 20 mM imidazole, 7 mM $\beta$-mercaptoethanol, 1%

triton X-100), wash buffer 1 [25 mM HEPES (pH 7.3), 300 mM NaCl, 0.1 mM EGTA, 3 mM $MgCl_2$, 40 mM imidazole], and wash buffer 2 [25 mM HEPES (pH 7.3), 500 mM NaCl, 0.1 mM EGTA, 3 mM $MgCl_2$, 65 mM imidazole]. The protein was eluted using an imidazole gradient (100–850 mM) and dialyzed against 25 mM HEPES (pH 7.3), 400 mM NaCl, 1 mM EGTA, 1 mM EDTA, 1 mM DTT, and 3% trehalose. After gel filtration (column Superdex 26/60–200 prep grade, Amersham Pharmacia), the protein was supplemented with 10% trehalose, flash frozen, and stored at −80°C.

Active site titration in the absence of F-actin using mantATP as a substrate was employed to determine the concentration of active myosin motors. The active motor concentration was typically ~50%. Concentrations reported in figure legends and throughout the text are final active-site concentrations. Rabbit skeletal muscle actin was prepared as described by Lehrer and Kerwar [21] and labeled with pyrene iodoacetamide as described previously by Criddle et al. [22]. TRITC-phalloidin labeling was carried out as reported [23].

## Enzyme kinetics

Steady-state kinetics were performed at 25°C with the NADH-coupled assay in a buffer containing 25 mM HEPES (pH 7.4), 5 mM $MgCl_2$, 0.5 mM DTT, 0.2 mM NADH, and an ATP regeneration system consisting of 0.05 mg/ml PK, 0.5 mM PEP, 0.02 mg/ml LDH, and 2 mM ATP. The myosin concentration was 0.15–0.5 μM. The F-actin concentration was varied between 0 and 100 μM. NADH oxidation was followed using the change in the absorption at 340 nm ($\varepsilon = 6220\ M^{-1}\ cm^{-1}$) in a temperature-controlled plate reader (MULTISKAN FC, Thermo) using UV-transparent microtiter plates. The ATPase activity in the absence of F-actin was subtracted from the actin-activated data.

Stopped-flow techniques were employed to study the interaction of myosin with nucleotides and F-actin. Stopped-flow measurements were conducted at 20°C with a Hi-tech Scientific SF-61SX2 stopped-flow system equipped with a 75 W mercury-xenon arc lamp in MOPS buffer [25 mM MOPS (pH 7.0), 100 mM KCl]. Magnesium concentrations were adjusted by supplementing $MgCl_2$ to the MOPS buffer. Free $Mg^{2+}$ ion concentration was calculated using the Maxchelator software as described previously [24].

Pyrene fluorescence was excited at 365 nm and monitored through a KV389 cutoff filter. Intrinsic tryptophan fluorescence was excited at 297 nm, and emission was selected using a WG320 cutoff filter. Mant nucleotides were excited either directly at 365 nm or excited via energy transfer from tryptophan (excitation at 297 nm),

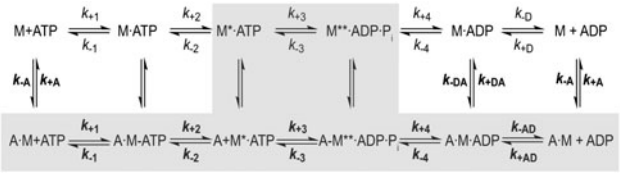


**Scheme 1**

and the emitted light was detected after passage through a KV389 cutoff filter. Changes in light scattering were monitored at 90° to the incident light by using an excitation wavelength of 320 nm. Data storage and initial fitting were performed using the software Kinetic Studio 1.08 (TgK Scientific). Unless stated otherwise, the reactant concentrations stated throughout the text are those after 1:1 mixing in the stopped-flow spectrophotometer. Analysis of kinetic data was accomplished using the same basic models that were developed to describe the kinetic behavior of rabbit fast skeletal muscle myosins and other myosins based on that of Bagshaw et al. [25–28]. Consistent with these models, kinetic parameters for the interaction of M7a with nucleotide and F-actin were analyzed in terms of the kinetic model shown in Scheme 1 [28, 29]. The abbreviations used are as follows: A = F-actin, M = myosin, $P_i$ = inorganic phosphate. The predominant flux of the reaction pathway is highlighted in grey. Rate constants are referred to as $k_{+n}$ and $k_{-n}$, respectively. Dissociation equilibrium constants are denoted as $K_n$. Bold notation ($\boldsymbol{K_n}$, $\boldsymbol{k_{+n}}$) represents the kinetic constants in the presence of F-actin. Subscript A and D refer to actin and ADP, respectively. $\boldsymbol{K_A}$ represents the affinity of myosin for F-actin, $\boldsymbol{K_D}$ the affinity of ADP for myosin, $\boldsymbol{K_{AD}}$ the affinity of ADP for the actomyosin complex, and $\boldsymbol{K_{DA}}$ the affinity of actin for myosin in the presence of saturating [ADP]. The asterisk (*) symbol represents changes in fluorescence intensity.

## Myosin motor activity

Actin-sliding motility was measured as described previously [30] in buffer containing 25 mM imidazole (pH 7.4), 25 mM KCl, 1 mM $MgCl_2$, 1 mM EGTA, 4 mM ATP, and an oxygen scavenging system consisting of 0.1 mg/ml glucose oxidase, 0.02 mg/ml catalase, and 5 mg/ml glucose. The experiment was performed at 30°C controlled by an enclose box on an Olympus IX70 microscope. The speed of actin filament sliding was tracked with the help of the program DiaTrack 3.01 (Semasopht, Switzerland). Data analysis was performed with Origin 8.0 (OriginLab, USA). Goodness-of-fit criteria were evaluated using the coefficient of determination $R^2$ and $\chi^2$ tests as implemented in Origin 8.0.

## Results

### Design, expression, and purification of human myosin-7a motor domain construct

To examine the enzymatic and mechanical properties of the myosin-7a motor, we designed and produced a recombinant construct containing the catalytically active human myosin-7a motor domain fused to an artificial lever arm and an EYFP fluorescence marker. The artificial lever arm comprises two spectrin-like repeats from *Dd* α-actinin and functionally replaces the native light chain-binding region [30]. This protein engineering approach directly links the myosin core region to the artificial lever arm, resulting in the production of the single-headed, constitutively active myosin constructs with similar kinetic and functional properties compared to S1-like myosin constructs [30–32]. Crystallographic and functional studies show that the artificial lever arm used in the present study forms a rigid and elongated structure that can functionally replace the native myosin lever arm [32, 33]. The fact that the myosin motor domain constructs bearing artificial lever arms can be produced and purified in large amounts makes them ideally suited for systematic studies of the structure, kinetics, and function of myosin motors from a wide range of classes and organisms [24, 31, 33–36]. In the case of the human myosin-7a motor domain construct M7a, the presence of the EYFP fluorescence marker attached to the C-terminus of the artificial lever arm led to a further tenfold increase in purification yields.

### Steady-state ATPase activity

We measured the basal ATPase activity of M7a as a function of [ATP] in the presence of an ATP-regenerating system. The plot of the observed ATPase rate versus [ATP] varies hyperbolically with the nucleotide concentration and gives a plateau value of 0.05 ± 0.01 $s^{-1}$ that corresponds to $k_{basal}$. Half-maximal activation occurred at 11.69 ± 1.77 μM ATP (Fig. 1a and Table 1). In the presence of saturating [F-actin], the ATPase activity of M7a displays a hyperbolic dependence on [ATP] and gives a value of 0.35 ± 0.01 $s^{-1}$ for the maximum activity ($k_{cat,ATP}$) with half-saturation occurring at 62.65 ± 7.09 μM ($K_{ATP}$).

Figure 1b depicts the actin-activated ATPase activity of M7a as a function of [F-actin]. A hyperbolic fit to the data set gives a maximum actin-activated ATPase activity ($k_{cat}$) of 0.35 ± 0.03 $s^{-1}$. Half-maximal activation ($K_{app,actin}$) occurred at an F-actin concentration of 8.3 ± 2.6 μM. The apparent second order rate constant for F-actin binding ($k_{cat}/K_{app,actin}$) is 0.04 ± 0.02 $\mu M^{-1}$ $s^{-1}$ (Table 1). Comparable values of the [F-actin] dependence of the steady-state ATPase were reported previously [37] and are summarized together with the determined constants of the present study in Table 1.

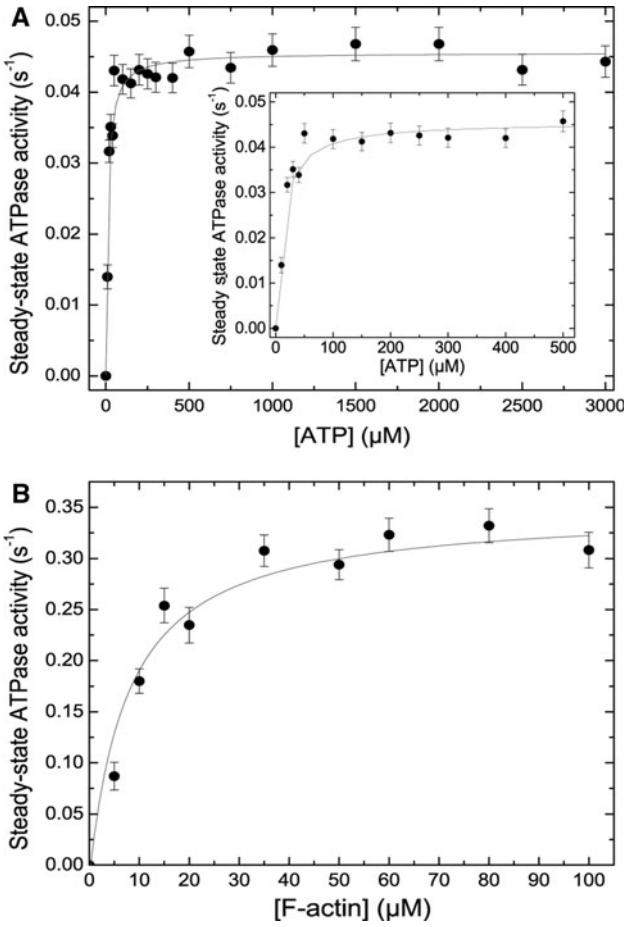


**Fig. 1** Steady-state ATPase activity. **a** Dependence of the basal steady-state ATPase activity of the myosin-7a motor on [ATP]. A hyperbolic fit to the data set (ATPase activity = ($k_{basal}$[ATP])/($K_{app,actin}$ +[ATP])) gives a value for maximal ATPase turnover ($k_{basal}$) as 0.05 ± 0.01 $s^{-1}$. *Inset*, close-up view of the data in the concentration range between 0 and 500 μM ATP. **b** Dependence of the steady-state ATPase activity of the human myosin-7a motor domain as a function of [F-actin]. The solid curve is a hyperbolic fit (ATPase activity = ($k_{cat}$[F-actin])/($K_{app,actin}$ + [F-actin])) giving $k_{cat}$ and $K_{app,actin}$ values of 0.35 ± 0.03 $s^{-1}$ and 8.3 ± 2.6 μM, respectively. The displayed data for the actin-activated steady-state ATPase activity are corrected for the basal ATPase activity. Error bars in panels A and B represent standard deviations from at least 6 determinations of each data point. The experimental conditions were as follows: 25 mM HEPES (pH 7.4), 5 mM $MgCl_2$, 0.5 mM DTT, and 2 mM ATP in the presence of an ATP regeneration system at a temperature of 25°C

### Actin interaction

Binding of the M7a construct to pyrene-labeled F-actin quenches the pyrene fluorescence. The transient decrease of pyrene fluorescence upon mixing M7a with pyrene-actin in a stopped-flow spectrophotometer follows a mono-exponential

**Table 1** Comparison of the steady-state parameters of the ATPase activity of human myosin-7a with rodent and *Drosophila* class 7 myosins

| Michalelis-Menten parameters | Signal or calculation | *Hs* Myosin-7a[d] | *Hs* Myosin-7a [37] | *Mm* Myosin-7a[e] [47] | *Dm* Myosin-7a [48] | *Dm* Myosin-7a [42] | *Rn* Myosin-7a [49] | *Dm* Myosin-7b [50] | *Mm* Myosin-7b [46] |
|---|---|---|---|---|---|---|---|---|---|
| $k_{basal}$ ($s^{-1}$) | NADH assay | 0.05 ± 0.01 | 0.05 ± 0.01 | 0.18 ± 0.02 | 0.05 ± 0.001 | 0.057 ± 0.041 | 0.04 | 0.020 | 0.02–0.03 |
| $k_{cat}$ ($s^{-1}$) | NADH assay | 0.35 ± 0.03[a] | 0.45 ± 0.05 | 0.7 ± 0.02 | 1.0 ± 0.1 | 1.72 ± 0.12 | 0.53 | 8.5 ± 0.6 | 1.17 ± 0.03 |
| $K_{app,actin}$ (μM) | NADH assay | 8.3 ± 2.6[a] | 12.8 ± 2.9 | 10.5 ± 1.7 | 1.1 ± 0.1 | 3.2 ± 1.1 | 32.7 | 39 ± 5 | 0.66 ± 0.01 |
| $k_{cat}/K_{app,actin}$ ($\mu M^{-1} s^{-1}$) | $k_{cat}/K^{b}_{app,actin}$ | 0.04 ± 0.02 | 0.04 ± 0.01 | 0.07 ± 0.01 | 0.91 ± 0.17 | 0.54 ± 0.22 | 0.02 | 0.22 ± 0.04 | 1.77 ± 0.06 |
| $k_{cat}/K_{app,actin}$ ($\mu M^{-1} s^{-1}$) | $k_{cat}/K^{c}_{app,actin}$ | 0.02 ± 0.01 | n.d. | n.d. | n.d. | n.d. | n.d. | n.d. | n.d. |
| $K_{ATP}$ (μM) | NADH assay | 11.69 ± 1.77 | n.d. | n.d. | n.d. | n.d. | 154 | n.d. | n.d. |
| $K_{ATP}$ (μM) | NADH assay | 62.65 ± 7.09 | n.d. | n.d. | n.d. | n.d. | 231 | n.d. | n.d. |
| $k_{cat,ATP}$ ($s^{-1}$) | NADH assay | 0.35 ± 0.01 | n.d. | n.d. | n.d. | n.d. | 0.46 | n.d. | n.d. |

[a] Values for $k_{cat}$ and $K_{app,actin}$ were calculated by fitting the data to a hyperbolic equation

[b] The apparent second order rate constant for F-actin binding ($K_{app,actin}$) was obtained from the calculated ratio of both values

[c] The apparent second order rate constant for F-actin binding ($K_{app,actin}$) was obtained from the initial slope

[d] Experimental conditions: 25 mM HEPES (pH 7.4), 5 mM $MgCl_2$, 0.5 mM DTT, 2 mM ATP in the presence of an ATP regeneration system

[e] Values in the presence of calmodulin

decay (Fig. 2a, *inset*). A secondary plot of the observed rate constants ($k_{obs}$) against the pyrene-actin concentration shows a linear dependence. This is compatible with a simple one-step binding process, where $k_{obs} = [A]\ \boldsymbol{k_{+A}} + \boldsymbol{k_{-A}}$ (Scheme 1) [38]. The value for the second order rate constant of pyrene-actin binding $\boldsymbol{k_{+A}}$ is given by the slope of the plot as 3.17 ± 0.06 $\mu M^{-1}\ s^{-1}$. The intercept, $\boldsymbol{k_{-A}}$, was too small to deduce an accurate value. In the presence of ADP, the rate of actin binding is reduced more than tenfold for many myosins [28]. When we performed the experiment with M7a in the presence of saturating concentrations of ADP, the $k_{obs}$ values were reduced but only to a smaller extent. In this case $k_{obs} = [A]\ \boldsymbol{k_{+DA}} + \boldsymbol{k_{-DA}}$. The slope obtained from the corresponding secondary plot of the data indicates a threefold reduction in the rate of actin binding (Fig. 2a).

Determination of the rate constants of M7a dissociation from pyrene-labeled F-actin in the absence ($\boldsymbol{k_{-A}}$) and presence ($\boldsymbol{k_{-DA}}$) of saturating ADP (250 μM) was measured by chasing pyrene-actin with an excess of unlabeled F-actin. The observed processes could be fit to single exponentials where $k_{obs}$ corresponds directly to the rates of actin dissociation with values of 0.002 ± 4 × $10^{-5}$ $s^{-1}$ for $\boldsymbol{k_{-A}}$ and 0.003 ± 1 × $10^{-4}$ $s^{-1}$ for $\boldsymbol{k_{-DA}}$. A typical time course for the dissociation from pyrene-labeled F-actin in the presence of ADP is shown in Fig. 2b. In the absence of ADP, the ratio of the experimentally determined binding and dissociation rate constants ($\boldsymbol{k_{-A}/k_{+A}}$) gives a value of 0.63 nM for the dissociation equilibrium constant for F-actin binding ($\boldsymbol{K_A}$). In the presence of ADP, the affinity of M7a for F-actin ($\boldsymbol{K_{DA} = k_{-DA}/k_{+DA}}$) is 2 nM.

## ATP binding to myosin-7a and ATP-induced dissociation of actomyosin-7a

We monitored binding of ATP to the M7a by the enhancement of intrinsic tryptophan fluorescence following the addition of excess ATP. A 5% increase in fluorescence is observed with M7a. The observed process could be fit to a single exponential [$F = F_\infty\ (1 - e^{-k_{obs}t})$]. The observed rate constants measured at different ATP concentrations are linearly dependent on the concentration of ATP up to 20 μM, with the slope defining an apparent second order binding constant $K_1k_{+2}$ of 0.85 ± 0.02 $\mu M^{-1}\ s^{-1}$. At higher ATP concentrations, up to a maximum of 0.5 mM, this dependence can be fit to a hyperbola ($k_{obs} = k_{max}$ [ATP]/([ATP] + $K_{0.5}$)), saturating at a rate of 23.34 ± 0.74 $s^{-1}$ (Fig. 3a). $K_{0.5}$ in this case simply defines the ATP concentration at which $K_1k_{+2}$ [ATP] approximately equals $(k_{+3}+k_{-3})/2$. In fact, if ATP binding is rapid and irreversible, as expected by analogy with *Dd* myosin-2 or skeletal muscle subfragment-1, a hyperbolic function is not expected (Scheme 1). The good fit to a hyperbola is partly due to the small change in fluorescence observed on ATP

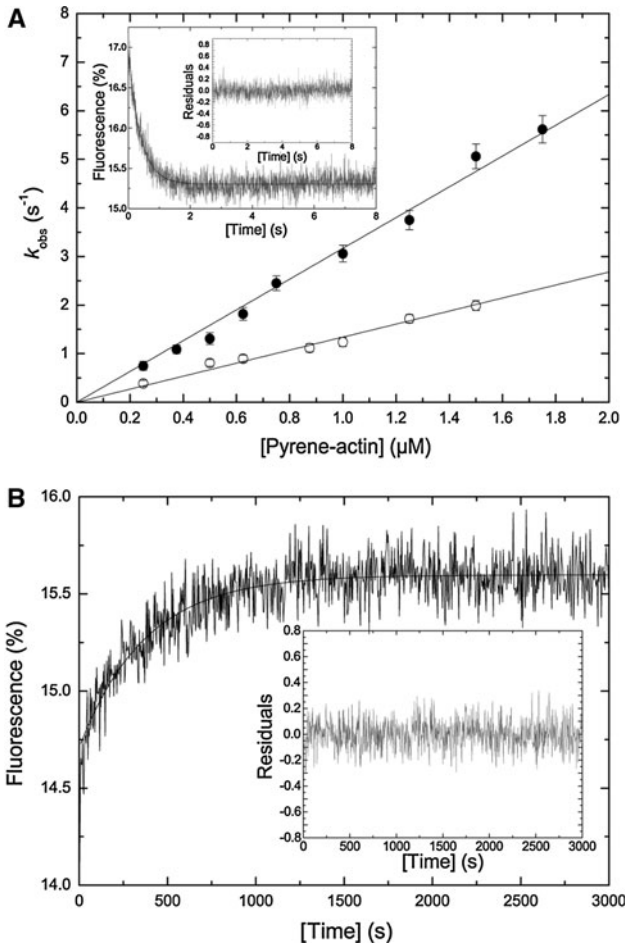


**Fig. 2** Interaction of the myosin-7a motor with F-actin in the absence of nucleotide and in the presence of ADP. **a** Binding of the human myosin-7a motor domain to pyrene-actin filaments in the absence (*filled circle*) and presence (*open circle*) of saturating ADP (250 μM). The concentration of the M7a construct was kept at 1:5 to 1:7.5 of the pyrene-actin concentration. The rate of pyrene-actin quenching is linearly dependent on [pyrene-actin] up to 1.75 μM. The apparent second order rate constants derived from the slopes of linear fits to the data sets are $\boldsymbol{k_{+A}} = 3.17 \pm 0.06\ \mu M^{-1}s^{-1}$ and $\boldsymbol{k_{+DA}} = 1.34 \pm 0.03\ \mu M^{-1}s^{-1}$, respectively. *Inset*, time course upon mixing M7a (0.125 μM) with an excess of pyrene-actin (0.75 μM) approximated with a single exponential equation. Time axes are identical for the data fits and the corresponding residual plot. *Error bars* represent standard deviations from at least three determinations of each data point. **b** Chase experiment of the ternary pyrene-acto•M7a•ADP complex (0.25 μM) with excess of unlabeled F-actin (20 μM). A single exponential fit to the transient shown gives a value for $\boldsymbol{k_{-DA}}$ as $0.003 \pm 1.10^{-4}\ s^{-1}$. Time axes in the data fit and the corresponding residual plot (*inset*) are the same. Experimental conditions were as follows: 20°C, 25 mM MOPS (pH 7.0), 100 mM KCl, 5 mM $MgCl_2$, and 10 mM DTT. Nucleotide-free samples were prepared by preincubation of the reactants with 0.1 U/ml apyrase for 15 min at room temperature

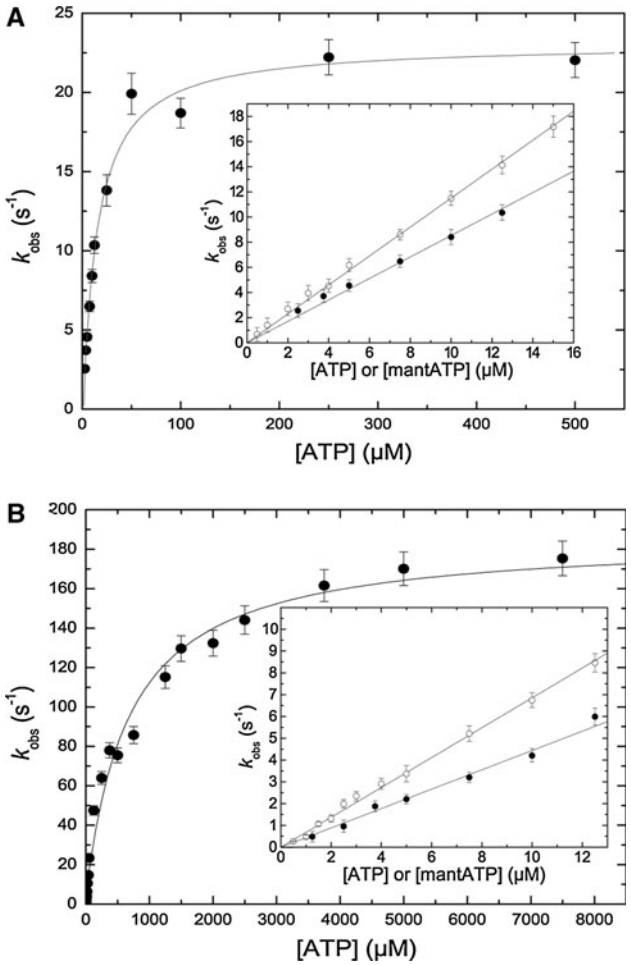


**Fig. 3** ATP binding to myosin-7a motor and ATP-induced dissociation of actomyosin-7a. **a** ATP binding to myosin-7a motor was followed in a stopped-flow apparatus by the change in intrinsic fluorescence signal. A plot of the observed rate constants versus [ATP] shows a hyperbolic dependence converging at a rate of $k_3 + k_{-3} = 23.1 \pm 0.74\ s^{-1}$. *Inset*, ATP binding to myosin-7a motor monitored by tryptophan and mantATP fluorescence. Rate of ATP (*filled circle*) and mantATP (*open circle*) binding to myosin-7a motor domain as a function of nucleotide concentration. The solid lines correspond to the linear fit of the initial slopes and define the second order rate constant for ATP ($K_1k_{+2} = 0.85 \pm 0.02\ \mu M^{-1}\ s^{-1}$) and mantATP ($K_1k_{+2} = 1.15 \pm 0.01\ \mu M^{-1}\ s^{-1}$) binding to the myosin-7a motor. **b** ATP-induced dissociation of the preformed actomyosin-7a complex. Light-scattering transients were obtained by mixing actomyosin-7a with varying [ATP] under pseudo-first order conditions. A hyperbolic fit to the data set converges $\boldsymbol{k_{+2}} = 186 \pm 5.7\ s^{-1}$ with half-saturating ATP concentration $1/\boldsymbol{K_1} = 681.19 \pm 5.63\ \mu M$. *Inset,* ATP (*filled circle*) and mantATP (*open circle*) binding to actomyosin-7a. The apparent second order binding rate constants ($\boldsymbol{K_1k_{+2}}$) were deduced from the slopes of the linear approximations and are listed in Table 2. *Error bars* in panels **a** and **b** represent standard deviations from at least three determinations of each data point

binding for M7a. As the hyperbolic fit probably has no real meaning, only the second order rate constants at low ATP concentrations and the plateau values are quoted in Table 2. For *Dd* myosin-2 the plateau has been assigned to the rate constant for the conformational change that limits the ATP cleavage step ($k_{+3}$+$k_{-3}$) and the second order rate constant to $K_1k_{+2}$ [25, 28, 39]. We assume the same assignment holds for M7a.

**Table 2** Transient kinetic parameters of the actomyosin-7a ATPase cycle with corresponding values for rodent and *Drosophila* class 7 myosins

| Parameter | Signal or calculation | *Hs* Myosin-7a | *Mm* Myosin-7a [47] | *Dm* Myosin-7a [48] | *Dm* Myosin-7a [42] | *Dm* Myosin-7b [50] | *Mm* Myosin-7b [46] |
|---|---|---|---|---|---|---|---|
| $K_1k_{+2}$ ($\mu M^{-1}s^{-1}$) | mantATP | 1.15 ± 0.01 | 2.5 ± 0.04 (dmATP) | n.d. | 3.4 ± 0.2 | 3.4 ± 0.1 (dmATP) | 1.8 ± 0.1 |
| | Tryptophan | 0.85 ± 0.02 | 2.2 | n.d. | 2.6 ± 0.2 | 4.7 | 4.1 ± 0.9 |
| $\boldsymbol{K_1k_{+2}}$ ($\mu M^{-1}s^{-1}$) | Light scattering | 0.44 ± 0.01 | n.d. | 1.6 (pyrene signal) | 0.35 ± 0.04 | n.d. | 1.4 ± 0.1 |
| | mantATP | 0.68 ± 0.01 | 0.53 ± 0.04 (dmATP) | 1.0 ± 0.1 (dmATP) | 0.47 ± 0.02 | 2.2, 0.46 | |
| $1/\boldsymbol{K_1}$ ($\mu M$) | Light scattering | 681.19 ± 5.63 | 295 ± 42 | 93 | n.d. | n.d. | 646 ± 100 |
| $\boldsymbol{k_{+2}}$ ($s^{-1}$) | Light scattering | 186 ± 5.70 | 350 ± 19 | 148 ± 27 | >200 | >400, >50 (pyrene-actin) | 729 ± 46 |
| $k_3 + k_{-3}$ ($s^{-1}$) | Tryptophan | 23.1 ± 0.74 | 11.5 ± 0.83 | 10.6 ± 0.4 | 12.6 ± 0.9 | 160 ± 30 | 318 ± 23 |
| $k_{+D}$ ($\mu M^{-1}s^{-1}$) | mantADP | 0.98 ± 0.05 | 1.2 ± 0.06 (dmADP) | n.d. | 3.7 ± 0.1 | 2.3 ± 0.1 (dmADP) | 3.1 ± 0.1 |
| $k_{-D}$ ($s^{-1}$) | mantADP | 0.27 ± 0.01[a] | | n.d. | 1.8 ± 0.3 | 9.0 ± 0.2 (dmADP) | 4.5 ± 1.6 |
| | mantADP | 0.20 ± 0.01[b] | 2.1 ± 0.07 (dmADP) | n.d. | 2.3 ± 0.1 | 10.1 ± 0.7 (dmADP) | |
| | Tryptophan | 0.30 ± 0.002 | n.d. | n.d. | n.d. | n.d. | |
| $K_D$ ($\mu M$) | Tryptophan | 0.52 ± 0.09 | 3.5 (dmADP)[e] | n.d. | n.d. | n.d. | 0.2 ± 0.05 |
| | $k_{-D}/k_{+D}$ | 0.27 ± 0.03 | 1.75 (dmADP) | n.d. | 0.62 ± 0.03 | 3.8 | 1.3 ± 0.5 |
| $\boldsymbol{k_{+AD}}$ ($\mu M^{-1}s^{-1}$) | mantADP | 1.78 ± 0.04 | 1.5 ± 0.09 (dmADP) | 3.9 ± 0.1 (dmADP) | 4.7 ± 0.2 | 2.7 ± 0.4 (dmADP) | 3.4 ± 0.2 |
| $\boldsymbol{k_{-AD}}$ ($s^{-1}$) | mantADP | 0.59 ± 0.03[a] | n.d. | n.d. | 2.3 ± 0.5 | 16 ± 1 (dmADP) | 7.0 ± 2.2 |
| | Light scattering | 0.48 ± 0.01[b] | 1.28 ± 0.09 (ADP) | 7.7 ± 0.8 (pyrene data) | 1.86 ± 0.03 | 9.8 ± 3.5 (pyrene-actin) | n.d. |
| | mantADP | 0.32 ± 0.01[b] | 1.7 ± 0.2 (dmADP) | 7.8 ± 2.3 (dmADP) | 2.1 ± 0.5 | 9.6 ± 1.3 (dmADP) | 6.9 ± 0.1 |
| $K_i$ ($Mg^{2+}_{free}$) (mM) | mantADP | 0.29 ± 0.03[b] | n.d. | n.d. | n.d. | n.d. | n.d. |
| $\boldsymbol{K_{AD}}$ ($\mu M$) | $\boldsymbol{k_{-AD}/k_{+AD}}$ | 0.30 ± 0.22 (mantADP) | 1 (dmADP) | n.d. | 0.48 ± 0.127 | 3.6-5.9 (dmADP) | 2 |
| Coupling* | $\boldsymbol{K_{AD}}/K_D$ | ~1.2 | ~0.3–0.6 | n.d. | ~0.8 | ~0.7–1.6 | ~10 |
| Coupling** | $\boldsymbol{k_{-AD}}/k_{-D}$ | ~1.1–1.8 | ~0.6–0.8 | n.d. | ~1 | ~1.6 | ~1.5 |
| $\boldsymbol{k_{+A}}$ ($\mu M^{-1}s^{-1}$) | Pyrene-actin | 3.17 ± 0.06[d] | 4.7 ± 0.25 (light scattering) | n.d. | 0.88 ± 0.03 | 1.2 ± 0.1 | 12.1 ± 2.7 |
| $\boldsymbol{k_{-A}}$ ($s^{-1}$) | Pyrene-actin | 0.002 ± 4·10$^{-5}$ [d] | n.d. | n.d. | <0.0043 | 0.042 | 0.054 ± 0.0002 |
| $\boldsymbol{K_A}$ (nM) | $\boldsymbol{k_{-A}/k_{+A}}$ | 0.63 ± 0.02 | n.d. | n.d. | 4.8 | 35 | 4.5 ± 1.0 |
| $\boldsymbol{k_{+DA}}$ ($\mu M^{-1}$ $s^{-1}$) | Pyrene-actin | 1.34 ± 0.03[d] | 2.6 ± 0.25 (light scattering) | n.d. | 0.32 ± 0.02 | 1.0 ± 0.1 | 16.3 ± 6.0 |
| $\boldsymbol{k_{-DA}}$ ($s^{-1}$) | Pyrene-actin | 0.003 ± 1·10$^{-4}$ [d] | n.d. | n.d. | <0.03 | 0.034 | 0.043 ± 0.0001 |
| $\boldsymbol{K_{DA}}$ (nM) | $\boldsymbol{k_{-DA}/k_{+DA}}$ | 2 ± 0.13 | n.d. | n.d. | 94 | 34 | 2.6 ± 1.0 |
| Coupling*** | $\boldsymbol{K_{DA}/K_A}$ | ~3.17 | n.d. | n.d. | ~19.5 | ~0.97 | ~0.57 |
| Duty ratio | | ~0.6[c] | 0.6 | 0.88 | ~0.9 | ~0.8 | ~0.8 |

Numbering of the kinetic rates and constants correspond to Scheme 1. Experimental conditions were as follows if not stated otherwise: 25 mM MOPS (pH 7.0), 100 mM KCl, and 5 mM $MgCl_2$

* Thermodynamic coupling relating the affinity of ADP for actomyosin with the affinity of ADP for myosin

** ADP release rate enhancement by F-actin

*** Thermodynamic coupling relating the affinity of F-actin for myosin·ADP with the affinity of F-actin for myosin

[a] Ordinate of the $k_{obs}$ versus [mantADP] plot

[b] ATP-chase experiment

[c] 5 mM $MgCl_2$, as calculated from duty ratio = $((1/\boldsymbol{k_{-AD}}) + (1/\boldsymbol{k_{+2}}))/(1/k_{cat})$

[d] MOPS buffer supplemented with 10 mM DTT

[e] Single turnover data

Alternatively, binding of the substrate mantATP was monitored from the 2.3-fold increase in fluorescence observed upon addition of substoichiometric concentrations of mantATP to the myosin-7a motor domain construct. The observed process was analyzed as described for ATP binding, giving a similar second order rate constant $K_1k_{+2}$ of 1.15 ± 0.01 $\mu M^{-1}$ $s^{-1}$ from the initial slope (Fig. 3a, *inset* and Table 2).

The ATP-induced population of weakly bound acto•M7a states was determined by monitoring the decrease in the light-scattering signal. The process was modeled as a two-step binding reaction [40]. The time courses of the reduction in light scattering intensity follow single exponentials with an additional lag phase. As depicted in Fig. 3b, the [ATP]-dependence of the observed rate constants was fit to a hyperbola as predicted from Scheme 1. The maximum rates of dissociation measured allow the determination of the rate constant for the fast isomerization process $\boldsymbol{k_{+2}}$ of 186 ± 5.7 $s^{-1}$. The half-maximal rate of dissociation was reached at 681.19 ± 5.63 μM ATP and represents the apparent equilibrium constant for ATP binding ($1/\boldsymbol{K_1}$). The rate constant for ATP binding to the rigor complex ($\boldsymbol{K_1k_{+2}}$) was determined at low [ATP] by following the change in the intensity of light scattering. The observed rate constants depend linearly on the [ATP] up to 12.5 μM. The apparent second order binding rate constant $\boldsymbol{K_1k_{+2}}$ of 0.44 ± 0.01 $\mu M^{-1}$ $s^{-1}$ was deduced from the slope of a linear regression (Fig. 3b, *inset*). Additionally, we used the increase in the fluorescence intensity of the nucleotide analogue mantATP to determine the rate constants of ATP binding to acto•M7a. When mantATP was mixed with the rigor complex, a $\boldsymbol{K_1k_{+2}}$ of 0.68 ± 0.01 $\mu M^{-1}$ $s^{-1}$ was derived from the initial slope (Fig. 3b, *inset*).

## ADP binding to myosin-7a in the presence and absence of F-actin

To investigate ADP binding to myosin-7a, we used the fluorescent nucleotide analogue mantADP. Binding of mantADP to myosin was performed under pseudo first-order conditions by mixing myosin (0.125 μM) with varying concentrations of mantADP in a stopped-flow apparatus. The time course of the binding reaction was monitored by observing the exponential increase in fluorescence. The observed rate constants are linearly dependent on [mantADP] over the range from 0.5–4.5 μM. The slope of the plot shown in Fig. 4a gives a second order binding rate constant $k_{+D}$ of 0.98 ± 0.05 $\mu M^{-1}$ $s^{-1}$. The dissociation rate constant $k_{-D} = 0.27 \pm 0.01$ $s^{-1}$ was deduced from the ordinate intercept.

Mixing of 0.125 μM acto•M7a with excess amounts of mantADP resulted in fluorescence signals that could be fitted with a double-exponential function. Over the concentration range from 0.5–10 μM, the observed rate constant for the fast phase is linearly dependent on the concentration of nucleotide. In contrast, amplitude and rate do not change over the same range for the slow phase. As the slow phase makes only a minor contribution to the overall signal and due to its invariance, we have not considered it during data analysis. Linear approximations of the data of the fast phase give an apparent second order rate constant $\boldsymbol{k_{+AD}}$ of 1.78 ± 0.04 $\mu M^{-1}s^{-1}$ (Fig. 5a). Extrapolation of the line to zero [mantADP] indicates a dissociation rate constant $\boldsymbol{k_{-AD}}$ of 0.59 ± 0.03 $s^{-1}$.



**Fig. 4** ADP interaction. **a** mantADP binding to the myosin-7a motor domain. A linear approximation of the data set gives the second order rate constant $k_{+D} = 0.98 \pm 0.05$ $\mu M^{-1}$ $s^{-1}$. *Inset*, time course of mantADP (1 μM) binding to M7a (0.125 μM) in a stopped-flow apparatus. A single exponential fit to the time course gives $k_{obs} = 1.37$ $s^{-1}$. The corresponding residual plot has the same time axes as the fit. **b** ADP release from M7a. Time course of the change in fluorescence intensity for the displacement of ADP (500 μM) from 0.25 μM with 1,500 μM ATP in the stopped-flow apparatus. The change in intrinsic tryptophan fluorescence was fitted using a single exponential function, giving a value of 0.3 ± 0.002 $s^{-1}$ for $k_{-D}$. The residual plot (*inset*) and the fit have the same time axes. **c** Competitive binding of ATP and ADP to M7a. The time course in the absence of ADP was fitted by a single exponential function, whereas the time courses in the presence of ADP were fit to bi-exponentials. The dependence of the observed amplitudes of the slow phase increases with increasing [ADP]. A hyperbolic fit of the data set resulted in a $K_D$ of 0.52 ± 0.09 μM. *Error bars* represent standard deviations from at least three determinations of each data point

## ADP dissociation from myosin-7a in the absence and presence of F-actin

The rate of ADP dissociation from myosin was measured by monitoring the decrease in fluorescence upon displacement of mantADP from M7a with excess ATP. A single-exponential approximation to the observed decrease in the fluorescence signal gives a rate constant $k_{-D}$ of 0.20 ± 0.01 $s^{-1}$ (data not shown). Alternatively, we followed the dissociation of the M7a•ADP complex by the displacement of ADP with excess ATP. A single-exponential approximation to the observed increase in the intrinsic protein fluorescence signal gives a rate constant $k_{-D}$ of 0.300 ± 0.002 $s^{-1}$ (Fig. 4b).

We determined the rate of displacement of ADP from acto•M7a by monitoring the exponential decrease of the light scattering signal that follows the addition of excess ATP. A value of 0.48 ± 0.01 $s^{-1}$ was obtained for the dissociation rate constant $\boldsymbol{k_{-AD}}$ (Fig. 5b). Alternatively, the dissociation rate constant was determined by chasing the preincubated acto•M7a•mantADP complex with excess ATP and following the monophasic decrease in the fluorescence signal. A value of 0.32 ± 0.01 $s^{-1}$ was obtained for the $\boldsymbol{k_{-AD}}$ using this approach (data not

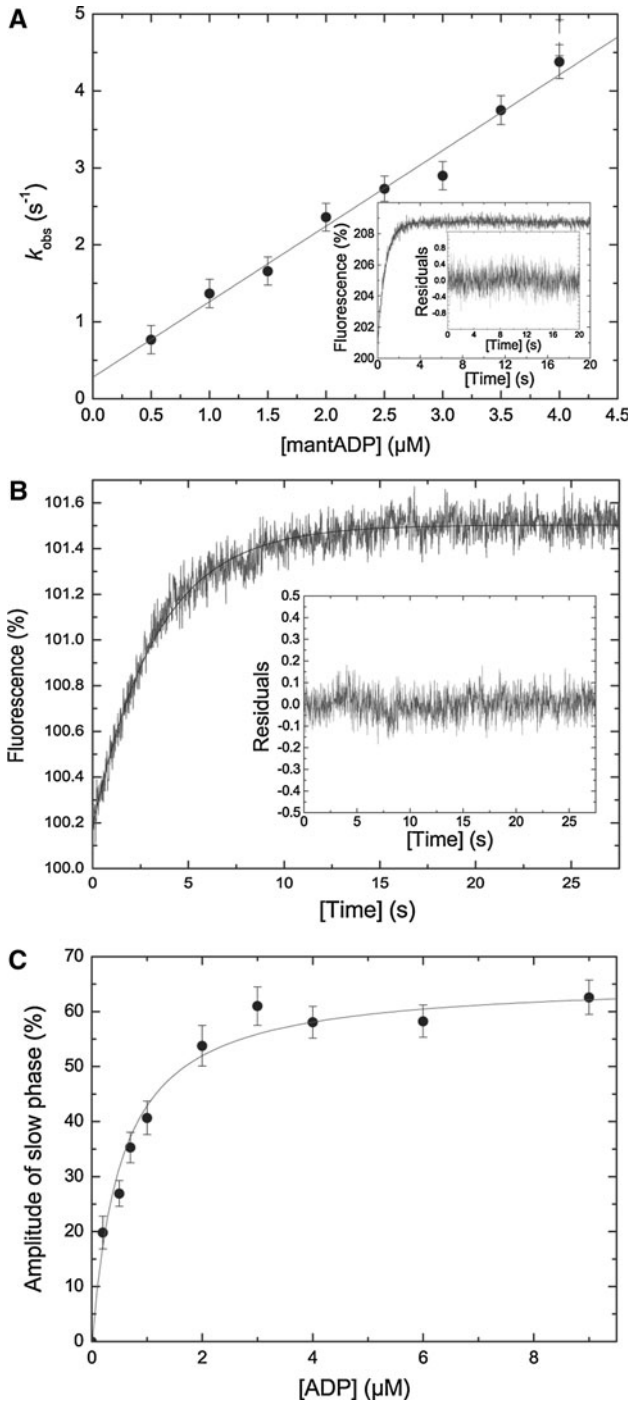


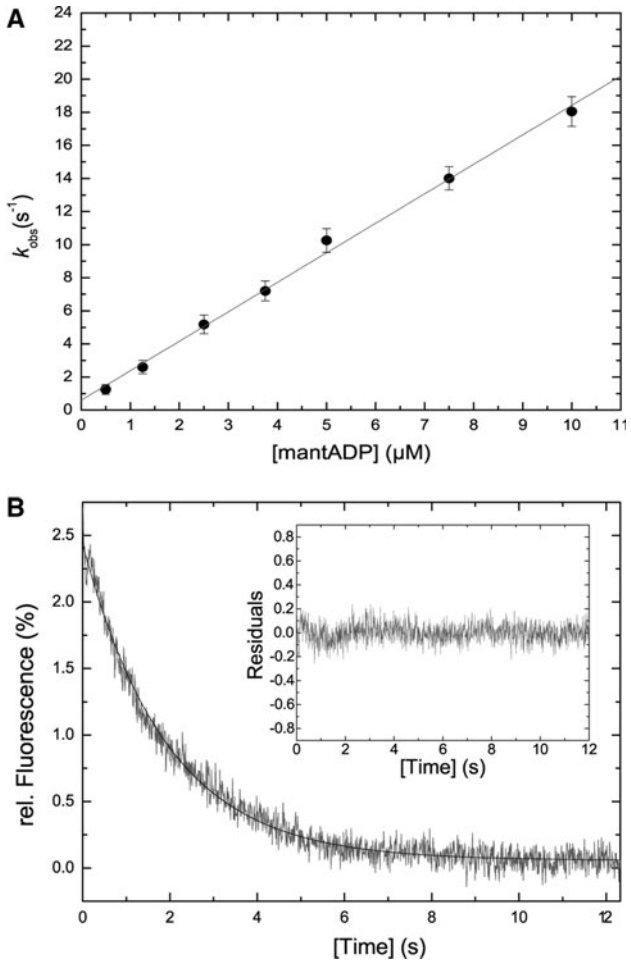


**Fig. 5** ADP interaction of acto•M7a. **a** ADP binding to acto•M7a. Linear approximation of the data set gives the second order rate constant of mantADP binding to actomyosin-7a $\boldsymbol{k_{+AD}} = 1.78 \pm 0.04\ \mu M^{-1}\ s^{-1}$. The corresponding intercept defines $\boldsymbol{k_{-AD}} = 0.59 \pm 0.03\ s^{-1}$. *Error bars* represent standard deviations from at least three determinations of each data point. **b** ADP dissociation from acto•M7a. Displacement of ADP (1 μM) from 0.25 μM acto•M7a with excess ATP (1,000 μM). Single exponential approximation of the decrease in light scattering signal gives $\boldsymbol{k_{-AD}} = 0.48 \pm 0.01\ s^{-1}$. The corresponding residual plot (*inset*) comprises the same time axes as the data fit

shown). The determined rate constants are in good agreement and similar to those reported previously by Watanabe and coworkers [37] (Table 2). As the kinetics of ADP binding and release are not greatly changed in the presence of saturating concentrations of F-actin ($k_{+D} \approx \boldsymbol{k_{+AD}}$; $k_{-D} \approx \boldsymbol{k_{-AD}}$), the thermodynamic coupling between the affinity of myosin for ADP and F-actin ($\boldsymbol{K_{AD}}/K_D \approx 1.2$) is weak (Table 2). The value of $\boldsymbol{k_{-AD}}$ is close to the maximum steady-state cycling rate in the presence of saturating F-actin ($k_{cat}$), indicating that this step is rate limiting in the pathway ($k_{cat} \approx \boldsymbol{k_{-AD}}$).

## ADP affinity in the presence and absence of F-actin

The dissociation equilibrium constant for ADP binding to actomyosin ($\boldsymbol{K_{AD}}$) was calculated to be $0.3 \pm 0.22$ μM from the ratio of the binding and dissociation rate constants $\boldsymbol{K_{AD} = k_{-AD}/k_{+AD}}$. By analogy, the dissociation equilibrium constant in the absence of F-actin $K_D = 0.27 \pm 0.03$ μM was calculated from the ratio $k_{-D}/k_{+D}$. An experimental method of determining $K_D$ is the displacement of ADP from myosin by the addition of

excess ATP. Similar to the behavior of *Dd* myosin-2 [41], ATP binding to M7a produces a larger increase in the intensity of the intrinsic protein fluorescence signal than binding of ADP. In the assay, myosin was preincubated with increasing concentrations of ADP and rapidly mixed with ATP. The change of the intrinsic fluorescence signal was mono-exponential in the absence of ADP. In the presence of ADP, the observed fluorescence transients were biphasic and could be described by double-exponential fits. This behavior is compatible with a kinetic model in which the amplitude of the fast phase represents ATP binding to free myosin, whereas the amplitude of the slow phase is governed by the release of ADP from M•ADP. As [ADP] was increased, the observed relative amplitude of the slow phase increased. The [ADP] dependence of the relative amplitude of the slow phase ($A_{slow}/A_{slow} + A_{fast}$) on [ADP] is hyperbolic, giving the dissociation equilibrium constant $K_D = 0.52 \pm 0.09$ μM (Fig. 4c).

### Magnesium sensitivity

Changes in the concentration of free $Mg^{2+}$ ions affect the ADP release kinetics from actomyosin. The observed rate constants for the displacement of ADP from acto•M7a by competition with ATP show a sigmoidal dependence on the concentration of free $Mg^{2+}$ ions (Fig. 6a). Increasing the level of free $Mg^{2+}$ ions within the range from 0.01 to 19 mM reduces the apparent rate of ADP release about fivefold from 0.92 to 0.20 $s^{-1}$. The apparent inhibition constant $K_i = 0.29 \pm 0.03$ mM lies within the intracellular range of free $Mg^{2+}$-ion concentrations. In agreement with our previous interpretation of the data, indicating that ADP release from actomyosin is the rate-limiting step in the actomyosin ATPase cycle, $Mg^{2+}$ sensitivity defines the actin-activated steady-state ATPase activity of human myosin-7a in a dose-dependent manner. As depicted in Fig. 6b, $Mg^{2+}$ deprivation increased the steady-state turnover 3.5-fold. The inhibitory constant $K_i$ is 291 μM, corresponding to the value determined from the ADP release experiments.

### Myosin-7a motor activity

The functional competence of the recombinant myosin motor domain construct was demonstrated in the in vitro motility assay [23]. Analysis of the velocity of fluorescent-labeled actin filaments over a myosin-decorated glass surface gives a mean velocity of ~97 nm $s^{-1}$ at free $Mg^{2+}$-ion concentrations smaller than 0.2 mM. Filament movement ceases completely at concentrations of free $Mg^{2+}$ greater than 1 mM (data not shown).

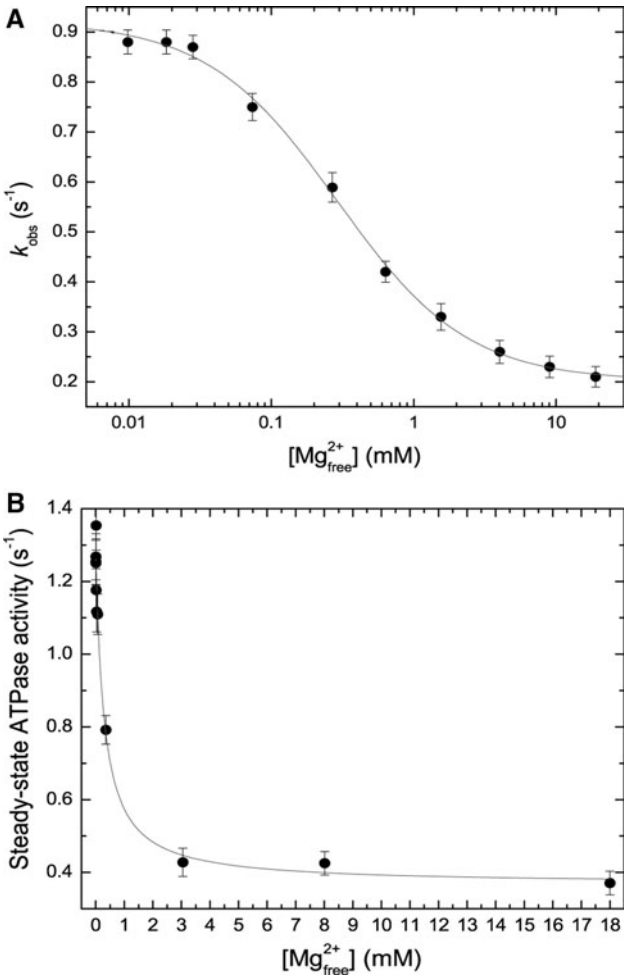


**Fig. 6** $Mg^{2+}$ sensitivity of acto•M7a. (**A**) Inhibition of the rate of ADP dissociation from acto•M7a by free $Mg^{2+}$. Increasing the concentration of free $Mg^{2+}$ ions within the range between 0.01 and 19 mM suppresses ADP release kinetics fivefold with a $K_i = 0.29 \pm 0.03$ mM. The data were fitted to the following equation $\boldsymbol{k_{-AD}} = (k_{min} \cdot (Mg^{2+}/K_i) + k_{max})/((Mg^{2+}/K_i) + 1)$. **b** Inhibitory effect of free $Mg^{2+}$ ions on the actin-activated steady-state ATPase activity at 40 μM F-actin. The data set was fitted to a hyperbolic function resulting in a $K_i$ of 0.29 mM. *Error bars* represent standard deviations from at least three determinations of each data point

## Discussion

Here, we describe in detail the kinetic and functional properties of the human myosin-7a motor domain. A defining feature of the myosin-7a actin-activated ATPase cycle is the rate-limiting ADP release step. This is indicative for the time the motor spends in the strongly bound actomyosin·ADP state and hence a high duty ratio. The thermodynamic coupling of ADP and F-actin binding or the extent to which saturating concentrations of F-actin accelerate the release of ADP defines the specific adaptation of a myosin for its particular cellular function. In case of myosin-7a, the coupling between actin and nucleotide

binding ($\boldsymbol{K_{AD}}/K_D \sim 1.2$) is weak. Consistently, ADP release is weakly accelerated in the presence of F-actin ($\boldsymbol{k_{-AD}}/k_{-D} \sim 1.1$–$1.8$). Under the assumption that human myosin-7a has a load-dependent ADP release, the kinetic properties are compatible with myosin-7a acting as tension sensor, as defined by Nyitrai and Geeves [29].

Table 2 summarizes the kinetic constants of human myosin-7a together with those from rodent and *Drosophila* orthologues. The comparison of human myosin-7a with other class-7 orthologues shows that all myosin-7 motors display slow ATP turnover in combination with a high affinity for F-actin. An exceptional case is *Drosophila* myosin-7b, which shows both, a faster steady-state ATPase and lower affinity for F-actin in the presence and absence of ADP. As listed in Table 1, the coupling efficiency between the nucleotide binding site and the F-actin binding region ($k_{cat}/K_{app,\ actin}$) is low for human, mouse, and rat myosin-7a (96–97% sequence identity within the motor domain) and elevated for the *Drosophila* myosins-7a and -7b and murine myosin-7b (sequence identity 56–65% with the human myosin-7a motor domain). A rate-limiting ADP release step from actomyosin and high duty ratios seem to be common features of class-7 myosins from different species qualifying these motors to participate in tension-mediating processes (Table 2). Furthermore, a specific attribute of class-7a myosins is an up to 25-fold reduced ATP hydrolysis rate $k_3 + k_{-3}$ when compared with class 7b myosins. In this context, *Drosophila* myosin-7a is unique since it hydrolyzes ATP predominantly while bound to F-actin [42] (Table 2).

Kinetic studies performed with unconventional myosins from classes 1 and 5 revealed that the steady-state ATPase and ADP release rates are inhibited by free $Mg^{2+}$ in the upper physiological range, indicating that ADP leaves the catalytic site via a $Mg^{2+}$-dependent mechanism [24, 34, 43, 44]. Our results show that magnesium ions act as modulators of myosin-7a motor activity. Changes in the level of free $Mg^{2+}$ ions within the physiological range affect ADP release kinetics from actomyosin-7a. At low $Mg^{2+}$-ion concentrations, fast ADP dissociation occurs. High concentrations of free $Mg^{2+}$ slow the release of ADP and consequently stabilize the tension-bearing actomyosin·ADP state. Since ADP release is the rate-determining step in the ATPase cycle, excess free $Mg^{2+}$ ions do affect the steady-state turnover of ATP. The inhibitory constant of $K_i = 291$ μM lies in the lower range of cytosolic free $Mg^{2+}$ ion concentrations.

Assuming that changes in the concentration of free $Mg^{2+}$ ions affect primarily ADP release kinetics and to a much smaller extent ADP-binding kinetics, $\boldsymbol{K_{AD}}$ is magnesium sensitive and decreases with increasing $Mg^{2+}$. This assumption is in good agreement with the observation that the in vitro sliding velocity is $Mg^{2+}$ ion dependent. The $Mg^{2+}$ sensitive ADP release activity of myosin-7a resembles that found in other unconventional myosins. Previous studies proposed a model in which $Mg^{2+}$ ion sensitivity is relevant for myosins that display a strain-dependent ADP dissociation step associated with an additional movement of the lever arm [43, 45]. Henn and coworkers speculate that murine myosin-7b undergoes a rotation of the regulatory domain and a load-dependent ADP release [46]. Therefore, it is conceivable that the $Mg^{2+}$ ion sensitivity of human myosin-7a follows the same mechanism.

Taken together, the main properties of human myosin-7a are a rate-limiting and $Mg^{2+}$ ion-sensitive ADP-release step from actomyosin, high affinities for ADP and F-actin, and a low degree of coupling between the actin- and nucleotide-binding sites. These specific kinetic adaptations indicate that human myosin-7a is a slow molecular motor with a high duty ratio, suitable for moving cargoes and mediating tension in the cytoskeleton. Spatio-temporal fluctuations in the cytosolic concentration of free $Mg^{2+}$ ions are likely to enable this molecular motor to switch between cargo-moving and tension-bearing modes.

**Acknowledgments** We thank Krishna Chinthalapudi and Igor Chizhov for helpful discussions. The work was supported by grants from Deutsche Forschungsgemeinschaft Ma 1081/16-1 and the Cluster of Excellence "Rebirth" to D.J.M.



## References

1. Berg JS, Powell BC, Cheney RE (2001) A millennial myosin census. Mol Biol Cell 12:780–794
2. Hasson T, Heintzelman MB, Santos-Sacchi J, Corey DP, Mooseker MS (1995) Expression in cochlea and retina of myosin VIIa, the gene product defective in Usher syndrome type 1B. Proc Natl Acad Sci USA 92:9815–9819
3. Wolfrum U, Liu X, Schmitt A, Udovichenko IP, Williams DS (1998) Myosin VIIa as a common component of cilia and microvilli. Cell Motil Cytoskeleton 40:261–271
4. Sahly I, El-Amraoui A, Abitbol M, Petit C, Dufier JL (1997) Expression of myosin VIIA during mouse embryogenesis. Anat Embryol (Berl) 196:159–170
5. Chen ZY, Hasson T, Kelley PM, Schwender BJ, Schwartz MF, Ramakrishnan M, Kimberling WJ, Mooseker MS, Corey DP (1996) Molecular cloning and domain structure of human myosin-VIIa, the gene product defective in Usher syndrome 1B. Genomics 36:440–448
6. Weil D, Levy G, Sahly I, Levi-Acobas F, Blanchard S, El-Amraoui A, Crozet F, Philippe H, Abitbol M, Petit C (1996) Human myosin VIIA responsible for the Usher 1B syndrome: a predicted membrane-associated motor protein expressed in developing sensory epithelia. Proc Natl Acad Sci USA 93:3232–3237
7. Levy G, Levi-Acobas F, Blanchard S, Gerber S, Larget-Piet D, Chenal V, Liu XZ, Newton V, Steel KP, Brown SD, Munnich A,

Kaplan J, Petit C, Weil D (1997) Myosin VIIA gene: heterogeneity of the mutations responsible for Usher syndrome type IB. Hum Mol Genet 6:111–116
8. Yang Y, Baboolal TG, Siththanandan V, Chen M, Walker ML, Knight PJ, Peckham M, Sellers JR (2009) A FERM domain autoregulates Drosophila myosin 7a activity. Proc Natl Acad Sci USA 106:4189–4194
9. Soni LE, Warren CM, Bucci C, Orten DJ, Hasson T (2005) The unconventional myosin-VIIa associates with lysosomes. Cell Motil Cytoskeleton 62:13–26
10. Self T, Mahony M, Fleming J, Walsh J, Brown SD, Steel KP (1998) Shaker-1 mutations reveal roles for myosin VIIA in both development and function of cochlear hair cells. Development 125:557–566
11. Kros CJ, Marcotti W, van Netten SM, Self TJ, Libby RT, Brown SD, Richardson GP, Steel KP (2002) Reduced climbing and increased slipping adaptation in cochlear hair cells of mice with Myo7a mutations. Nat Neurosci 5:41–47
12. Adato A, Michel V, Kikkawa Y, Reiners J, Alagramam KN, Weil D, Yonekawa H, Wolfrum U, El-Amraoui A, Petit C (2005) Interactions in the network of Usher syndrome type 1 proteins. Hum Mol Genet 14:347–356
13. Liu X, Ondek B, Williams DS (1998) Mutant myosin VIIa causes defective melanosome distribution in the RPE of shaker-1 mice. Nat Genet 19:117–118
14. Gibbs D, Kitamoto J, Williams DS (2003) Abnormal phagocytosis by retinal pigmented epithelium that lacks myosin VIIa, the Usher syndrome 1B protein. Proc Natl Acad Sci USA 100:6481–6486
15. Liu X, Udovichenko IP, Brown SD, Steel KP, Williams DS (1999) Myosin VIIa participates in opsin transport through the photoreceptor cilium. J Neurosci 19:6267–6274
16. Wolfrum U, Schmitt A (2000) Rhodopsin transport in the membrane of the connecting cilium of mammalian photoreceptor cells. Cell Motil Cytoskeleton 46:95–107
17. Weil D, Blanchard S, Kaplan J, Guilford P, Gibson F, Walsh J, Mburu P, Varela A, Levilliers J, Weston MD et al (1995) Defective myosin VIIA gene responsible for Usher syndrome type 1B. Nature 374:60–61
18. Gibson F, Walsh J, Mburu P, Varela A, Brown KA, Antonio M, Beisel KW, Steel KP, Brown SD (1995) A type VII myosin encoded by the mouse deafness gene shaker-1. Nature 374:62–64
19. Hildebrand MS, Thorne NP, Bromhead CJ, Kahrizi K, Webster JA, Fattahi Z, Bataejad M, Kimberling WJ, Stephan D, Najmabadi H, Bahlo M, Smith RJ (2010) Variable hearing impairment in a DFNB2 family with a novel MYO7A missense mutation. Clin Genet 77:563–571
20. Knight PJ, Thirumurugan K, Xu Y, Wang F, Kalverda AP, Stafford WF, Sellers JR, Peckham M (2005) The predicted coiled-coil domain of myosin 10 forms a novel elongated domain that lengthens the head. J Biol Chem 280:34702–34708
21. Lehrer SS, Kerwar G (1972) Intrinsic fluorescence of actin. Biochemistry 11:1211–1217
22. Criddle AH, Geeves MA, Jeffries T (1985) The use of actin labelled with N-(1-pyrenyl)iodoacetamide to study the interaction of actin with myosin subfragments and troponin/tropomyosin. Biochem J 232:343–349
23. Kron SJ, Spudich JA (1986) Fluorescent actin filaments move on myosin fixed to a glass surface. Proc Natl Acad Sci USA 83:6272–6276
24. Dürrwang U, Fujita-Becker S, Erent M, Kull FJ, Tsiavaliaris G, Geeves MA, Manstein DJ (2006) Dictyostelium myosin-IE is a fast molecular motor involved in phagocytosis. J Cell Sci 119:550–558
25. Batra R, Geeves MA, Manstein DJ (1999) Kinetic analysis of Dictyostelium discoideum myosin motor domains with glycine-to-alanine mutations in the reactive thiol region. Biochemistry 38:6126–6134
26. Bagshaw CR, Eccleston JF, Eckstein F, Goody RS, Gutfreund H, Trentham DR (1974) The magnesium ion-dependent adenosine triphosphatase of myosin. Two-step processes of adenosine triphosphate association and adenosine diphosphate dissociation. Biochem J 141:351–364
27. De La Cruz EM, Ostap EM, Sweeney HL (2001) Kinetic mechanism and regulation of myosin VI. J Biol Chem 276:32373–32381
28. De La Cruz EM, Wells AL, Rosenfeld SS, Ostap EM, Sweeney HL (1999) The kinetic mechanism of myosin V. Proc Natl Acad Sci USA 96:13726–13731
29. Nyitrai M, Geeves MA (2004) Adenosine diphosphate and strain sensitivity in myosin motors. Philos Trans R Soc Lond B Biol Sci 359:1867–1877
30. Anson M, Geeves MA, Kurzawa SE, Manstein DJ (1996) Myosin motors with artificial lever arms. EMBO J 15:6069–6074
31. Kurzawa SE, Manstein DJ, Geeves MA (1997) *Dictyostelium discoideum* myosin II: characterization of functional myosin motor fragments. Biochemistry 36:317–323
32. Kliche W, Fujita-Becker S, Kollmar M, Manstein DJ, Kull FJ (2001) Structure of a genetically engineered molecular motor. EMBO J 20:40–46
33. Ruff C, Furch M, Brenner B, Manstein DJ, Meyhofer E (2001) Single-molecule tracking of myosins with genetically engineered amplifier domains. Nat Struct Biol 8:226–229
34. Taft MH, Hartmann FK, Rump A, Keller H, Chizhov I, Manstein DJ, Tsiavaliaris G (2008) Dictyostelium Myosin-5b is a conditional processive motor. J Biol Chem 283:26902–26910
35. Ito K, Kashiyama T, Shimada K, Yamaguchi A, Awata J, Hachikubo Y, Manstein DJ, Yamamoto K (2003) Recombinant motor domain constructs of Chara corallina myosin display fast motility and high ATPase activity. Biochem Biophys Res Commun 312:958–964
36. Kollmar M, Durrwang U, Kliche W, Manstein DJ, Kull FJ (2002) Crystal structure of the motor domain of a class-I myosin. EMBO J 21:2517–2525
37. Watanabe S, Umeki N, Ikebe R, Ikebe M (2008) Impacts of Usher syndrome type IB mutations on human myosin VIIa motor function. Biochemistry 47:9505–9513
38. Taylor EW (1991) Kinetic studies on the association and dissociation of myosin subfragment 1 and actin. J Biol Chem 266:294–302
39. Cremo CR, Geeves MA (1998) Interaction of actin and ADP with the head domain of smooth muscle myosin: implications for strain-dependent ADP release in smooth muscle. Biochemistry 37:1969–1978
40. Millar NC, Geeves MA (1983) The limiting rate of the ATP-mediated dissociation of actin from rabbit skeletal muscle myosin subfragment 1. FEBS Lett 160:141–148
41. Ritchie MD, Geeves MA, Woodward SK, Manstein DJ (1993) Kinetic characterization of a cytoplasmic myosin motor domain expressed in Dictyostelium discoideum. Proc Natl Acad Sci USA 90:8619–8623
42. Watanabe S, Ikebe R, Ikebe M (2006) Drosophila myosin VIIA is a high duty ratio motor with a unique kinetic mechanism. J Biol Chem 281:7151–7160
43. Rosenfeld SS, Houdusse A, Sweeney HL (2005) Magnesium regulates ADP dissociation from myosin V. J Biol Chem 280:6072–6079
44. Fujita-Becker S, Durrwang U, Erent M, Clark RJ, Geeves MA, Manstein DJ (2005) Changes in Mg2 + ion concentration and heavy chain phosphorylation regulate the motor activity of a class I myosin. J Biol Chem 280:6064–6071
45. Hannemann DE, Cao W, Olivares AO, Robblee JP, De La Cruz EM (2005) Magnesium, ADP, and actin binding linkage of

myosin V: evidence for multiple myosin V-ADP and actomyosin V-ADP states. Biochemistry 44:8826–8840
46. Henn A, De La Cruz EM (2005) Vertebrate myosin VIIb is a high duty ratio motor adapted for generating and maintaining tension. J Biol Chem 280:39665–39676
47. Haithcock J, Billington N, Choi K, Fordham J, Sellers JR, Stafford WF, White H, Forgacs E (2011) The Kinetic Mechanism of Mouse Myosin VIIa. J Biol Chem 286:8819–8828
48. Yang Y, Kovács M, Sakamoto T, Zhang F, Kiehart DP, Sellers JR (2006) Dimerized Drosophila myosin VIIa: a processive motor. Proc Natl Acad Sci USA 103:5746–5751
49. Inoue A, Ikebe M (2003) Characterization of the motor activity of mammalian myosin VIIA. J Biol Chem 278:5478–5487
50. Yang Y, Kovacs M, Xu Q, Anderson JB, Sellers JR (2005) Myosin VIIB from Drosophila is a high duty ratio motor. J Biol Chem 280:32061–32068